Probing electron transfer within alkali-metal halides via high-order harmonic generation

Michael Spanner and Paul Brumer
Chemical Physics Theory Group, Department of Chemistry, and Center for Quantum Information and Quantum Control, University of Toronto, Toronto, Canada M5S 3H6

(Received 19 November 2007; published 30 September 2008)

High-order harmonic generation (HHG) from an excited alkali-metal halide diatomic molecule undergoing electron transfer is considered. A clear signature of electron transfer, a result of a nonadiabatic coupling between the covalent and ionic electronic states, is seen in the HHG spectrum. This work demonstrates the feasibility of HHG probing of simple chemically relevant electronic dynamics, an approach capable of providing spatial and momentum structure regarding the electron transfer process.

DOI: 10.1103/PhysRevA.78.033840 PACS number(s): 42.65.Ky, 32.80.Wr, 34.70.+e

I. INTRODUCTION

Electron transfer stands as one of the fundamental processes in molecular physics and chemistry [1]. For example, it is an integral component of the harpoon mechanism, a basic mechanism in elementary molecular reaction dynamics [2], where electron transfer occurs at large internuclear distances. In this paper we propose, and computationally demonstrate, an experimentally feasible method of using high-order harmonic generation (HHG) to probe electron transfer dynamics within alkali-metal halides, with NaI used as a specific example. The method thereby extends high-order harmonic probing to chemically relevant electronic dynamics.

In high-order harmonic generation [3,4], a strong laser field ionizes an atom or molecule, accelerates the liberated electron to kinetic energies on the order of a few tens of eV, and drives the electron to recollide with the parent ion, all within a single optical cycle. Upon recollision, the electron can recombine with the ion, radiating its excess energy as a high-energy photon—the high-order harmonic emission. Due to its eV-range energy, the liberated electron recollides with a subangstrom wavelength, making the process extremely sensitive to the spatial structure of both the nuclei and the electronic orbitals of the parent ion. With respect to nuclear degrees of freedom, recent experiments have shown HHG to be a sensitive probe of vibrational [5] and rotational [6] dynamics in molecules. A striking example of the high sensitivity to electronic degrees of freedom is the recent experimental realization of orbital tomography using high-order harmonic emission, where the highest occupied molecular orbital (HOMO) orbital of N_2 was reconstructed from a series of high-order harmonic measurements [7], demonstrating that high-order harmonic probing carries great potential for exploring electronic states of molecules. Demonstration of the ability to explore electron transfer dynamics within alkali-metal halides, as shown here, greatly extends this capability. The present work builds toward methods capable of full time-dependent experimental characterization of the relevant electronic orbitals during an electron transfer process, motivating further work on complete orbital reconstruction.

The two lowest Born-Oppenheimer potential energy curves of alkali-metal halide diatomics display a generic characteristic. At large internuclear distances R, one potential curve corresponds to a covalent configuration $M+X$ while the other corresponds to the ionic configuration $M^+ + X^-$; the two curves cross as R becomes smaller. Figure 1(a) shows the covalent and ionic curves for the case of NaI [8]. When an alkali-metal halide in the ground electronic state at the equilibrium internuclear distance is photoexcited to the covalent state, the excited nuclear wave packet moves toward the crossing point, undergoing a nonadiabatic transition corresponding to electron transfer, i.e., the valence electron moves from the M atom of the $M+X$ species to the X atom to form $M^+ + X^-$. During the transfer, the electronic state is in a coherent superposition of electronic states. HHG emission from targets in coherent electronic superpositions was first studied with a focus on using the superposition state to tune and enhance the harmonic emission [9], and more recently with the intention of imaging the electronic motion [10]. The present study considers the interesting case where the elec-

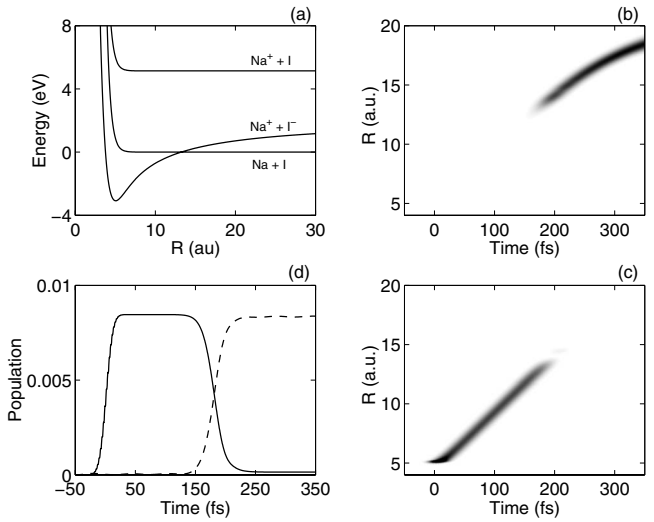

FIG. 1. Nonadiabatic electron transfer dynamics of the excited wave packet. Relevant potential energy curves for electron transfer in the NaI system are shown in (a). (b) and (c) plot $|\chi_I(R,t)|^2$ and $|\chi_C(R,t)|^2$, respectively, that is, the time-dependent radial probability distributions on the ionic and covalent surfaces. (White corresponds to zero probability, black corresponds to maximum probability.) (d) plots the electronic populations of the excited wave packet. Solid curve denotes the covalent state, dashed curve denotes the ionic state.

tronic coherence arises from the electronic-nuclear coupling present in alkali-metal halides.

Building on established techniques in strong field science, our proposed experiment for probing this electron transfer process would proceed as follows. Initially, a linearly polarized laser pulse is used to align the molecules along the direction of the laser polarization [11,12]. Below we assume that the molecules are perfectly aligned. (Indeed, field-free laser-induced alignment of NaI has been previously studied [13], and periods of strong alignment in field-free conditions lasting ~1 to 2 ps can be created.) A second pulse, arriving during a period of field-free alignment and polarized parallel to the molecular axis, is used to excite a vibrational wave packet on the covalent surface. To facilitate HHG probing of only the excited population, we envision pumping the vibrational wave packet in a grating configuration [14]. Such a configuration allows one to isolate subsequent emission from the excited wave packet through spatial diffraction, in analogy with standard four-wave mixing and transient grating techniques [15]. Finally, the HHG probe pulse is sent to probe the excited wave packet. In order to simplify the interpretation of the HHG signal, we use a HHG pulse polarized perpendicular to the molecular axis, minimizing additional electronic excitations induced by the HHG probe. As the HHG probe arrival time is varied with respect to the vibrational excitation pulse, the electronic dynamics and electron transfer of the excited wave packet can be monitored through the emitted HHG spectrum. We note that previous theoretical studies [16] have considered probing this covalent-to-ionic transition in NaI using time-resolved photoelectron spectroscopy. By comparison, the present method has considerable advantages insofar as it provides an all-optical technique to probe the nonadiabatic electronic dynamics and provides for the simultaneous probing of a large range of momentum components of the electronic orbitals.

II. THEORY

A. Nuclear dynamics

Consider NaI using the model and potential energy surfaces outlined in Ref. [8]. This model was successfully applied to the analysis of early NaI femtosecond experiments [17,18]. The pump laser pulse $E_p(t)$ is chosen to be

$$E_p(t) = \mathcal{E}_p \exp(-4 \ln 2 t^2/\sigma_p^2)\cos(\omega_p t). \tag{1}$$

With the pulse written in this way, σ_p is the full width at half maximum, and is set to $\sigma_p = 30$ fs. The maximum electric field strength and central frequency are $\mathcal{E}_p = 1.7 \times 10^{-4}$ a.u. (intensity of 10^9 W/cm^2) and $\omega_p = 0.1373$ a.u. (328 nm). Figure 1 shows the calculated nuclear dynamics following excitation of the ground vibrational state on the ionic surface by the pump pulse. Figures 1(b) and 1(c) plot the time-dependent radial probability distributions $|\chi_I(R,t)|^2$ and $|\chi_C(R,t)|^2$, respectively, where R is the vibrational coordinate and the C and I subscripts refer to the covalent and ionic electronic states, respectively. Figure 1(d) plots the time-dependent populations of both electronic states, $P_i(t) = \int dR |\chi_i(R,t)|^2$ $(i = I, C)$. Note that the initial ground state has been projected out of $\chi_I(R,t)$ before these results were plotted, in order to focus on the excitation portion of the total wave function. The nonadiabatic transition corresponding to electron transfer is clearly seen to occur over the range of 160–210 fs.

B. High-order harmonics

Consider now high-order harmonic generation from the excited nuclear wave packet. The vector potential and electric field of the HHG pulse are set to

$$A(t) = -\frac{\mathcal{E}_H}{\omega_H} \exp[-4 \ln 2 (t - t_d)^2/\sigma_H^2]\cos(\omega_H t) \tag{2}$$

and $E_H(t) = -\partial A(t)/\partial t$, where t_d is the time delay between the excitation pulse and the HHG probe pulse, and the pulse is assumed to be polarized perpendicular to the molecular axis. Since the NaI and Na^+I^- species have relatively low ionization potentials (~5.14 eV) we choose a carrier wavelength of $\omega_H = 0.0143$ a.u. (3200 nm) for the HHG pulse in order to increase the recollision energy as much as possible prior to saturation. In order to avoid excessive time-averaging of the transition during the probing step, we use a single-cycle pulse $\sigma_H = 2\pi/\omega_H$ (10.6 fs) with peak field strength of $\mathcal{E}_H = 0.02$ a.u. $(1.4 \times 10^{13}$ W/cm$^2)$.

The total wave function (vibrational and electronic) is written as

$$|\Psi_0(t)\rangle = |\chi_I(t)\rangle|\phi_I^{(n)}\rangle + |\chi_C(t)\rangle|\phi_C^{(n)}\rangle, \tag{3}$$

where $|\phi_j^{(n)}\rangle$ $(j = C, I)$ are n-electron states at the average bond length of the corresponding vibrational wave packet $|\chi_j(t)\rangle$. Note that the $|\phi_j^{(n)}\rangle$ are normalized eigenstates that depend parametrically on the average bond length, while the $|\chi_j(t)\rangle$ represent the time-dependent nuclear wave packets whose norms change as the vibrational wave packet moves from one surface to the other. The HHG problem is treated within a single active electron approach, where the strong field is assumed to act only on the liberated electron.

The strong field approximation (SFA) is used to described the ionization and continuum motion of the free electron [4,19]. The core approximation in the SFA is that, after ionization, the effect of the binding potential is neglected in the continuum electron dynamics. The free electron is then described by Volkov states [20], which are plane waves describing the free electron oscillating in the strong laser field. Although the SFA falls short of full quantitative prediction, it gives excellent qualitative insight and is sufficient to explore the main features of HHG probing of electron transfer in alkali-metal halides.

In addition to the SFA, we assume negligible depletion of the initial state during the HHG pulse, keep the nuclei frozen during the HHG process, and include only the lowest electronic surface of the Na^+I ion following strong field ionization from either the NaI or Na^+I^- state. With these assumptions, the dipole describing the HHG emission polarized perpendicular to the molecule is written, in atomic units $(\hbar = m_e = e = 1)$, as

$$d_{\mathrm{HHG}}(t) = -i\int_0^t dt' \int d\mathbf{k}\,\exp\left(-i\frac{1}{2}\int_{t'}^{t} d\tau[\mathbf{k}+\mathbf{A}(\tau)]^2\right)E_H(t')$$
$$\times[\langle\phi_I^{(n)}|\hat{r}_x|\phi^{(n-1)};\mathbf{k},t\rangle\langle\phi^{(n-1)};\mathbf{k},t'|\hat{r}_x|\phi_I^{(n)}\rangle$$
$$\times\langle\chi_I(t_d)|\chi_I(t_d)\rangle e^{-iI_{p,I}(t-t')} + \langle\phi_C^{(n)}|\hat{r}_x|\phi^{(n-1)};\mathbf{k},t\rangle$$
$$\times\langle\phi^{(n-1)};\mathbf{k},t'|\hat{r}_x|\phi_C^{(n)}\rangle\langle\chi_C(t_d)|\chi_C(t_d)\rangle e^{-iI_{p,C}(t-t')}$$
$$+\langle\phi_C^{(n)}|\hat{r}_x|\phi^{(n-1)};\mathbf{k},t\rangle\langle\phi^{(n-1)};\mathbf{k},t'|\hat{r}_x|\phi_I^{(n)}\rangle$$
$$\times\langle\chi_C(t_d)|\chi_I(t_d)\rangle e^{-iI_{p,C}t+iI_{p,I}t'} + \langle\phi_I^{(n)}|\hat{r}_x|\phi^{(n-1)};\mathbf{k},t\rangle$$
$$\times\langle\phi^{(n-1)};\mathbf{k},t'|\hat{r}_x|\phi_C^{(n)}\rangle\langle\chi_I(t_d)|\chi_C(t_d)\rangle e^{-iI_{p,I}t+iI_{p,C}t'}], \tag{4}$$

where $|\phi^{(n-1)};\mathbf{k},t\rangle \equiv |\phi^{(n-1)}\rangle|\mathbf{k},t\rangle$, $|\phi^{(n-1)}\rangle$ is the $(n-1)$-electron state of the ion, $|\mathbf{k},t\rangle$ are the single-electron plane wave continuum states defined as $\langle\mathbf{r}|\mathbf{k},t\rangle = (2\pi)^{-(3/2)}e^{i[\mathbf{k}+\mathbf{A}(t)]\cdot\mathbf{r}}$, and $\mathbf{r}$ is the spatial coordinate of the continuum electron. The ionization potentials are evaluated at the average bond length $\bar{R}_j(t_d)=\langle\chi_j(t_d)|\hat{R}|\chi_j(t_d)\rangle$, for each time delay

$$I_{p,j} = V_+(\bar{R}_j(t_d)) - V_j(\bar{R}_j(t_d)), \tag{5}$$

where $V_+(R)$ is the potential energy surface of Na^+I.

By neglecting exchange effects between the continuum and core electrons and by assuming no core rearrangement following ionization, the multielectron transition matrix elements are replaced by single-electron matrix elements

$$\langle\phi^{(n-1)};\mathbf{k},t|\hat{r}_x|\phi_j^{(n)}\rangle = \langle\mathbf{k},t|\hat{r}_x|\psi_j^H\rangle, \tag{6}$$

where $|\psi_j^H\rangle$ is the HOMO of the electronic state $|\phi_j^{(n)}\rangle$. Although this is a long-standing approximation used in HHG, recent studies of multielectron effects have rigorously shown that such models correctly capture the lowest-order effects [21,22]. Further, the HOMOs are approximated by the Na $3s$ valence state located at $\bar{R}_j(t_d)/2$ for the covalent configuration, and the I^- $5p$ state located at $-\bar{R}_j(t_d)/2$ for the ionic configuration, with the atomic valence orbitals taken from Ref. [23].

The first two terms in Eq. (4) represent the harmonic emission from each electronic state individually—they would appear in identical form for an incoherent mixture of the $|\chi_I(t)\rangle|\phi_I^{(n)}\rangle$ and $|\chi_C(t)\rangle|\phi_C^{(n)}\rangle$ states. The second two terms represent the interference between these two states arising from the coherence between them. Note, however, that due to the $\langle\chi_C(t)|\chi_I(t)\rangle$ factor in the interference terms, the coherence is manifest only when the nuclear wave packets overlap.

We evaluate Eq. (4) numerically, including all t' and $\mathbf{k}$ integration points. To accelerate the convergence of the highly oscillatory integrals we use the Filinov filter, common to the semiclassical initial value representation techniques [24]. When evaluating Eq. (4), both so-called "long" and "short" recollision trajectories are present. These are trajectories that ionize at different times but end up recolliding with the same energy. When both are present in the computations, interferences in the HHG spectra arise. However, the HHG emission from these two types of trajectories phase match differently, and either the long or short trajectories can be readily selected in experiments by tuning the focus of the HHG pulse relative to the generating medium. In order to avoid spurious long-short interference in the computation, which is routinely avoided experimentally, we include an additional temporal filter when calculating the HHG dipole $d_f(t)=f(t)d_{\mathrm{HHG}}(t)$, where $f(t)=1/2-\mathrm{erf}[(t-t_d-t_f)/\sigma_f]/2$ with $t_f=20$ fs and $\sigma_f=0.25$ fs. Figure 2(a) shows $f(t)$ plotted over a window Fourier transform representation of $d_{\mathrm{HHG}}(t)$ for $t_d=50$ fs, demonstrating that this choice of filter selects the short trajectories from the largest-energy recollision. The second recollision event, centered around $t=60$ fs in Fig. 2(a), is also cut by $f(t)$. However, this recollision event does not produce harmonics beyond about 35th order, and the details of interest discussed below pertain to the highest-order harmonics that result from the highest-energy recollision.

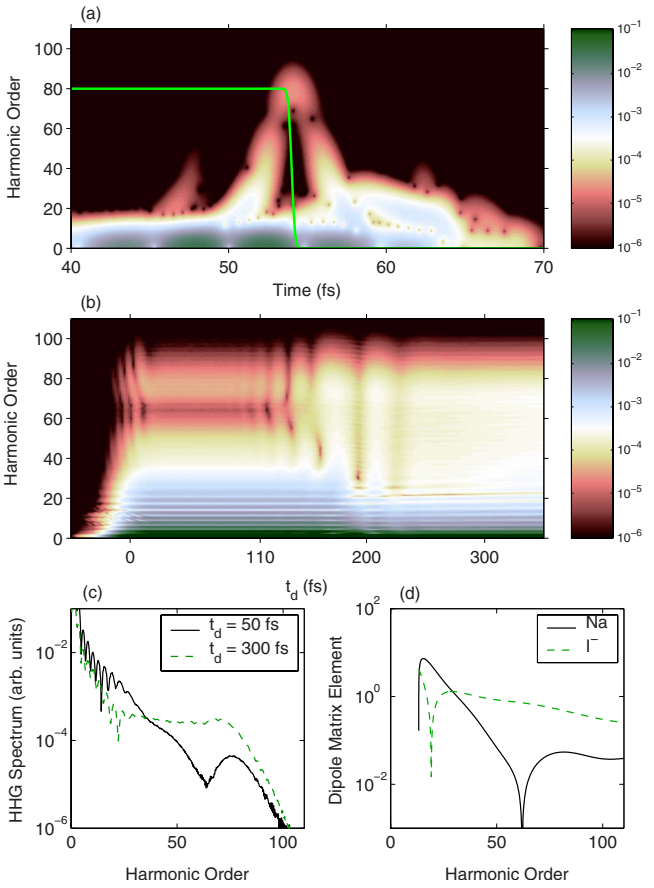

FIG. 2. (Color online) High-order harmonic spectra probing the electron transfer process. (a) Time-frequency representation of $d_{\mathrm{HHG}}(t)$ for $t_d=50$ fs. The solid curve shows the filter $f(t)$ for this delay. (b) HHG spectrum as a function of t_d. (c) HHG spectra for $t_d=50$ and 300 fs. (d) SFA recombination matrix elements plotted as a function of corresponding HHG emission energy E_{HHG}.

Figure 2 plots emitted t_d-dependent HHG specta as

$$|\mathcal{T}_{FF}[\partial^2 d_f(t)/\partial t^2]|^2/\omega^4 = |\omega^2\mathcal{T}_{FF}[d_f(t)]|^2/\omega^4 = |\mathcal{T}_{FF}[d_f(t)]|^2, \tag{7}$$

where $\mathcal{T}_F$ denotes the Fourier transform. Figure 2(b) plots the spectra for all delays, while Fig. 2(c) plots two representative

spectra taken at t_d=50 and 300 fs, before and after the electron transfer. Since we have used a single-cycle pulse, the highest-order harmonics result from a single-recollision wave packet and consequently display a continuous structure. Significantly, a large change in the HHG spectrum is seen to characterize the nuclear wave packet moving through the crossing region. The general character in the plateau region in Fig. 2(c) is largely governed by the recombination matrix element $\langle \psi_j^H | \hat{r}_x | \mathbf{k}, t \rangle$ in the last step of the HHG process. For small t_d, when the valence electron is located on the Na atom, the recolliding electron recombines with the Na 3*s* orbital, while at later times the recombination involves the 5*p* orbital of I^-. Figure 2(d) plots $\langle \psi_j^H | \hat{r}_x | \mathbf{k}, t \rangle$ for both valence orbitals as a function of the harmonic order using the SFA relation between emitted energy and recollision momentum, $E_{\mathrm{HHG}}=k^2/2+I_p$. The change in character of the harmonic emission is seen to directly reflect the change in the valence orbital structure. Although it is unclear if the pronounced dip at t_d=50 fs in the solid curve will survive the inclusion of Coulomb distortions in the recollision wave packet, which are present in an experiment but absent in the SFA, we expect that the change in the overall slope of the plateau will remain. Such a variation in the slope of the HHG plateau for varying atomic targets has been previously measured [25], and, due to the fact that the HOMOs are very atomiclike in alkali-metal halide systems, the analogous change of the slope seen in our calculations should be present in the experiment.

In addition to this change in character of the plateau region, interference beats are seen in Fig. 2(b) over the time interval where the nuclei pass through the crossing region, and readily provide a signature of the coherence present during the electron transfer process. The period of these interferences is seen to change as a function of t_d, a consequence of the fact that the phase of the interference terms in Eq. (4) is modulated by $I_{p,I}$, which varies as a function of t_d through Eq. (5). Thus, the variation of the ionization potential of the ionic states becomes encoded in the interference beats as the nuclear wave packet undergoes the nonadiabatic transition.

III. SUMMARY

This work demonstrates that HHG probing is capable of exposing the time-evolving dynamics of electron transfer within alkali-metal halides via the orbital structure and coherence during the electron transfer dynamics. The model used to describe the covalent-ionic crossing is deliberately simple, demonstrating the feasibility, and exploring the dominant qualitative features of, HHG probing of electron transfer in alkali-metal halides. Future studies can incorporate a more detailed description of the electronic states at the crossing point. This problem will also prove to be an important test case for inclusion of ionic core effects on the recollision electron [26]. The continuum electron liberated from the covalent configuration comes from the Na atom and will feel a Coulomb potential centered on its point of creation, while the electron liberated from the ionic configuration coming from the I^- will feel the Coulomb attraction of the Na^+, which is now shifted by a bond length from its point of creation, thus providing an interesting and clean test case for theories of Coulomb corrections in recollision physics that go beyond the plane wave description adopted in the SFA. Of further interest to chemical reaction dynamics would be, for example, the application of high-order harmonic probing to harpoon reactions triggered by laser excitation [27].

ACKNOWLEDGMENTS

M.S. thanks O. Smirnova for suggesting the use of a temporal filter. This work was supported by NSERC Canada.

[1] V. May and O. Kuhn, *Charge and Energy Transfer Dynamics in Molecular Systems* (Wiley-VCH, Weinheim, 2004).

[2] The harpoon mechanism is a long-range electron transfer process, typically between atoms or molecules with low ionization potentials interacting with molecules of high electron affinity, and often resulting in very large reaction cross sections. See M. Polanyi, *Atomic Reactions* (Williams and Norgate, London, 1932); D. R. Herschbach, in *Nobel Lectures, Chemistry 1981–1990*, editor in charge Tore Frängsmyr, edited by Bo G. Malmström (World Scientific Publishing, Singapore, 1992); R. D. Levine, *Molecular Reaction Dynamics* (Cambridge University Press, Cambridge, U.K., 2005).

[3] P. B. Corkum, Phys. Rev. Lett. **71**, 1994 (1993).

[4] M. Lewenstein, P. Balcou, M. Y. Ivanov, A. L'Huillier, and P. B. Corkum, Phys. Rev. A **49**, 2117 (1994).

[5] S. Baker, J. Robinson, C. A. Haworth, H. Teng, R. A. Smith, C. C. Chirila, M. Lein, J. W. G. Tisch, and J. P. Marangos, Science **312**, 424 (2006); N. L. Wagner, A. Wuest, I. P. Christov, T. Popmintchev, X. Zhou, M. M. Murnane, and H. C. Kapteyn, Proc. Natl. Acad. Sci. U.S.A. **103**, 13279 (2006).

[6] R. de Nalda, E. Heesel, M. Lein, N. Hay, R. Velotta, E. Springate, M. Castillejo, and J. P. Marangos, Phys. Rev. A **69**, 031804(R) (2004); J. Itatani, D. Zeidler, J. Levesque, M. Spanner, D. M. Villeneuve, and P. B. Corkum, Phys. Rev. Lett. **94**, 123902 (2005).

[7] J. Itatani *et al.*, Nature (London) **432**, 867 (2004).

[8] V. Engel and H. Metiu, J. Chem. Phys. **90**, 6116 (1989).

[9] J. B. Watson, A. Sanpera, X. Chen, and K. Burnett, Phys. Rev. A **53**, R1962 (1996); A. Sanpera, J. B. Watson, M. Lewenstein, and K. Burnett, *ibid.* **54**, 4320 (1996).

[10] H. Niikura, D. M. Villeneuve, and P. B. Corkum, Phys. Rev. Lett. **94**, 083003 (2005).

[11] P. W. Dooley, I. V. Litvinyuk, K. F. Lee, D. M. Rayner, M. Spanner, D. M. Villeneuve, and P. B. Corkum, Phys. Rev. A **68**, 023406 (2003).

[12] H. Stapelfeldt and T. Seideman, Rev. Mod. Phys. **75**, 543 (2003).

[13] M. Machholm, J. Chem. Phys. **115**, 10724 (2001).

[14] Y. Mairesse, D. Zeidler, N. Dudovich, M. Spanner, J. Levesque, D. M. Villeneuve, and P. B. Corkum, Phys. Rev.

Lett. **100**, 143903 (2008).
[15] S. Mukamel, *Principles of Nonlinear Optical Spectroscopy* (Oxford University Press, New York, 1995).
[16] Y. Arasaki, K. Takatsuka, K. Wang, and V. McKoy, Phys. Rev. Lett. **90**, 248303 (2003).
[17] T. S. Rose *et al.*, J. Chem. Phys. **88**, 6672 (1988).
[18] M. Grønager and N. E. Henriksen, J. Chem. Phys. **109**, 4335 (1998).
[19] L. V. Keldysh, Zh. Eksp. Teor. Fiz. **47**, 1945 (1964); F. H. M. Faisal, J. Phys. B **6**, L89 (1973); H. R. Reiss, Prog. Quantum Electron. **16**, 1 (1992).
[20] D. V. Volkov, Z. Phys. **94**, 250 (1935).
[21] R. Santra and A. Gordon, Phys. Rev. Lett. **96**, 073906 (2006).
[22] S. Patchkovskii, Z. Zhao, T. Brabec, and D. M. Villeneuve, Phys. Rev. Lett. **97**, 123003 (2006).
[23] Radzig and Smirnov, *Reference Data on Atoms, Molecules, and Ions* (Springer-Verlag, Berlin, 1985).
[24] M. Spanner and P. Brumer, J. Chem. Phys. **122**, 084111 (2005).
[25] J. Levesque, D. Zeidler, J. P. Marangos, P. B. Corkum, and D. M. Villeneuve, Phys. Rev. Lett. **98**, 183903 (2007).
[26] See, for example, O. Smirnova *et al.*, J. Phys. B **39**, S307 (2006), and references therein.
[27] P. Y. Cheng, D. Zhong, and A. H. Zewail, J. Chem. Phys. **103**, 5153 (1995).